Spine Deformity (2023) 11:59–69
https://doi.org/10.1007/s43390-022-00574-w

BIOMECHANICS

Proximal junctional failure after surgical instrumentation in adult spinal deformity: biomechanical assessment of proximal instrumentation stiffness

Maeva Lopez Poncelas[1,2] · Luigi La Barbera[1,2,3] · Jeremy Rawlinson[1,4] · Dennis Crandall[5,6,7] · Carl-Eric Aubin[1,2]

Received: 31 March 2022 / Accepted: 13 August 2022 / Published online: 9 September 2022

Abstract

Study design Assessment of different proximal instrumentation stiffness features to minimize the mechanical proximal junctional failure-related risks through computer-based biomechanical models.

Objective To biomechanically assess variations of proximal instrumentation and loads acting on the spine and construct to minimize proximal junctional failure (PJF) risks.

Summary of background data The use of less-stiff fixation such as hooks or tensioned bands, compared to pedicle screws, at the proximal instrumentation level are considered to allow for a gradual transition in stiffness with the adjacent levels, but the impact of such flexible fixation on the loads balance and complications such as PJF remain uncertain.

Methods Six patients with adult spine deformity who underwent posterior spinal instrumentation were used to numerically model and simulate the surgical steps, erected posture, and flexion functional loading in patient-specific multibody analyses. Three types of upper-level fixation (pedicle screws (PS), supralaminar hooks (SH), and sublaminar bands (SB) with tensions of 50, 250, and 350 N) and rod stiffness (CoCr/6 mm, CoCr/5.5 mm, Ti/5.5 mm) were simulated. The loads acting on the spine and implants of the 90 simulated configurations were analyzed using Kruskal–Wallis statistical tests.

Results Simulated high-tensioned bands decreased the sagittal moment at the adjacent level proximal to the instrumentation (1.3 Nm at 250 N; 2.5 Nm at 350 N) compared to screws alone (PS) (15.6 Nm). At one level above, the high-tensioned SB increased the sagittal moment (17.7 Nm-SB vs. 15.5 Nm-PS) and bending moment on the rods (5.4 Nm and 5.7 Nm vs. 0.6 Nm) ($p < 0.05$). SB with 50 N tension yielded smaller changes in load transition compared to higher tension, with moments of 8.1 Nm and 16.8 Nm one and two levels above the instrumentation. The sagittal moment at the upper implant–vertebra connection decreased with the rod stiffness (1.0 Nm for CoCr/6 mm vs. 0.7 Nm for Ti/5.5 mm; $p < 0.05$).

Conclusion Simulated sublaminar bands with lower tension produced smaller changes in the load transition across proximal junctional levels. Decreasing the rod stiffness further modified these changes, with a decrease in loads associated with bone failure, however, lower stiffness did increase the rod breakage risk.

Level of evidence N/A.

Keywords Biomechanical modeling · Proximal junctional failure · Adult spinal deformity · Sublaminar bands · Scoliosis

✉ Carl-Eric Aubin
Carl-Eric.Aubin@polymtl.ca

[1] Department of Mechanical Engineering, Polytechnique Montréal, Downtown Station, P.O. Box 6079, Montreal, QC H3C 3A7, Canada

[2] Research Center, Sainte-Justine University Hospital Center, 3175, Cote Sainte-Catherine Road, Montreal, QC H3T 1C5, Canada

[3] Department of Chemistry, Materials and Chemical Engineering "Giulio Natta", Laboratory of Biological Structure Mechanics, Politecnico di Milano, 32, Piazza Leonardo da Vinci, 32 20133 Milan, MI, Italy

[4] Spine Applied Research, Cranial and Spinal Technologies Medtronic, 18400 Pyramid Place, Memphis, TN 38132, USA

[5] Sonoran Spine Center, 1255 W Rio Salado Pkwy #107, Tempe, AZ 85281, USA

[6] Mayo Clinic, 5779 E Mayo Blvd, Phoenix, AZ 85054, USA

[7] University of Arizona School of Medicine, 475 N 5th St, Phoenix, AZ 85004, USA

Introduction

Spinal instrumentation and fusion surgery have become a common treatment to restore the balance in adult spinal deformity (ASD). Despite advances in surgical techniques and knowledge in spine biomechanics, postoperative complications are still a problem. Proximal junctional kyphosis (PJK) is one of the most frequent complications following long instrumentation. Measured on the sagittal radiograph between the inferior endplate of the upper instrumented vertebra (UIV) and the superior endplate of the vertebra two levels cranial to it [1], a proximal junctional angle (PJA) greater than 10° indicates a pathological kyphotic deformity of the adjacent segment. Yet, PJK can be asymptomatic and does not always require revision surgery. Proximal junctional failure (PJF) is a more severe form, potentially involving acute proximal collapse, junctional compression fracture, retrolisthesis and/or instrumentation failure such as rod breakage or screw loosening [2]. Revision surgery incidence following PJF is up to 47% [2] making it a clinical and economic issue. PJF pathomechanisms are multifactorial with multiple potential risk factors associated, for instance, with the magnitude of correction in the sagittal plane, the ligament disruption procedure or the type of implant used at the UIV [3, 4].

Compared to pedicle screws (PS), the use of a less-stiff fixation at the UIV, such as hooks or supplementary tensioned bands, are increasingly considered to allow for a gradual transition in stiffness between the instrumented spine and the non-instrumented adjacent levels [4]. Several biomechanical studies have evaluated the range of motion (ROM) transition offered with different instrumentation configurations and related PJF incidence [5] with varying findings. Hooks decreased the ROM of the adjacent segment [6], but not always significantly [7, 8]. Sublaminar tapes or bands can allow for a more effective transition in terms of ROM and intradiscal pressure [6, 7, 9]. The spine stiffness decreased at the adjacent segment with a less-stiff rod material [10], but not always [8]. Using lower diameter or transitional diameter rods was also reported to decrease the spinal loads and the ROM above UIV [10–12].

Despite the potential design advantages of more flexible rod-to-vertebra fixation to reduce the risk of PJF, it is still unclear how the different types of implants at UIV balance the loads between the anterior spine and instrumentation and affect the risk of PJF.

The purpose of this study was to compare different proximal instrumentation stiffnesses, including vertebra-to-rod types of fixation and rod characteristics, to test the hypothesis that more flexible proximal instrumentation would significantly reduce the load gradient (i.e., load changes) between the instrumented and uninstrumented spine, and the assumption that load change around UIV in the anterior spine and instrumentation might be a mechanical factor indicative of the risks associated with PJF.

Methods

Adult spinal deformity patients

With the approval of the Institutional Review Board, six ASD patients who underwent posterior spinal instrumentation surgery after 2017 were used to build the numerical biomechanical models to test the research hypothesis (Table 1). All the patients had developed a junctional subluxation complication (i.e., proximal junctional acute collapse) [13]

Table 1 Preoperative patients' demographic data and geometric indices

Case no	1	2	3	4	5	6
Sex	Female	Female	Female	Female	Female	Female
Age	84	75	68	66	55	77
Height (cm)	168	168	157	165	163	147
Weight (kg)	51	82	54	74	77	49
Pelvic incidence (°)	44	33	38	55	49	45
Pelvic tilt (°)	35	21	23	38	39	30
T4–T12 kyphosis (°)	41	46	34	29	25	30
L1–L5 lordosis (°)	13	14	4	35	10	12
SVA (mm)	66	− 31	10	− 61	8	60
Cobb angle of the main curvature (°)	41	10	35	3	19	13
End vertebrae	T11–L3	T6–T11	T11–L3	T9–L2	T4–L1	T11–L3
UIV	T10	T10	T9	T10	T10	T10
LIV	S1	S1	S1	S1	S1	S1

UIV/LIV upper/lower instrumented vertebra

without complications related to implant–bone interface and rod failure.

Multibody modeling and simulation

A patient-specific multibody spinal model, previously developed and validated to study PJF pathomechanisms, was used for this study [11, 12, 14, 15]. This model was based on the 3D geometry of the patients, built using vertebral and pelvic landmarks identified on preoperative lateral and coronal radiographs and 3D reconstruction techniques [16]. The multibody model was built using MD-ADAMS 2014 software (MSC Software Corp. Santa Ana, CA). It included vertebrae from C7 to L5 and the pelvis, which were considered as rigid bodies, interconnected with 6-dimensional general springs (e.g., 6-degree-of-freedom stiffness matrix) to globally represent the mechanical properties of each functional spinal unit (FSU) and components such as the ligaments, intervertebral disc, and facet joints. The mechanical properties of the FSU stiffness matrices were determined from reported biomechanical tests [17, 18]. The FSU stiffness matrices were thereafter adapted to represent the removal of posterior elements at the levels where osteotomies were performed as documented in the operation report [19].

Multiaxial pedicle screws (PS) were modeled as rigid bodies for the threaded shaft and screw head, connected by a revolute joint to represent the multiaxial motion. The PS shank was connected to the vertebral pedicle by a nonlinear spring representing the mechanical properties of its anchorage with the bone [15, 20]. The initial shape of the rods was defined from the postoperative radiographs and a calibration algorithm was performed to find their initial unloaded shape, so that following the simulation of the correction of the instrumentation in the erect position, the elastically deformed rods corresponded to those in the reference postoperative radiographs [21]. According to the surgical steps, moments and forces were applied progressively to correct the deformity and the rods were aligned in the implant heads. Cylindrical joints were then set between implant heads and the rods. After the simulation of all correction maneuvers, the rod–implant cylindrical joints were replaced by fixed joints to simulate the tightening of the set screws.

The supralaminar hooks (SH) were modeled as rigid bodies, with a nonlinear lamina-to-hook joint representing the compliant junction between the anchor and the vertebra, as described in a previous study [11].

The sublaminar bands (SB) were modeled as two parts. The SB clamp was considered as a rigid body linked to the rod with a cylindrical joint. The band was modeled as a unidirectional spring between the clamp and the vertebra lamina with a stiffness of 410 N/mm [22]. A tensioning force (between 50 and 350 N) was applied to tighten the band, and then the cylindrical joint was replaced with a fixed joint.

The intraoperative prone position was modeled with the pelvis fixed in space and an inline longitudinal joint at the C7 vertebra. The main correction maneuvers were simulated following the operation report for each case (Fig. 1). The

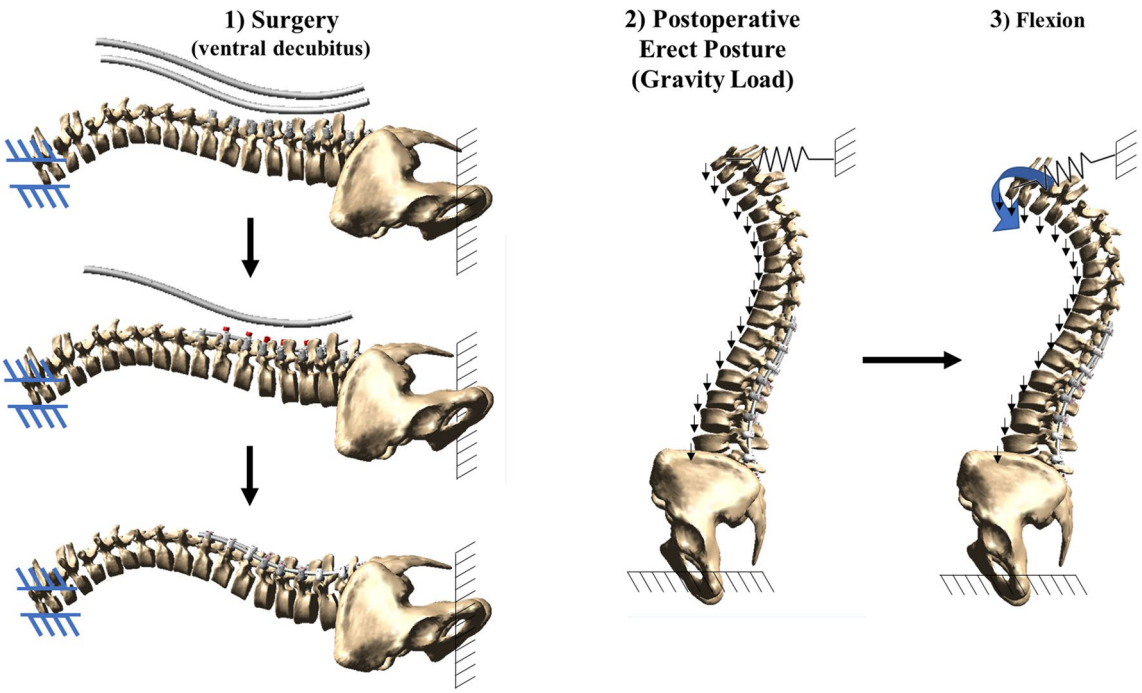

Fig. 1 Simulation main steps: (1) instrumentation in ventral decubitus position, (2) postoperative erected posture, and (3) flexion movement

erected postoperative posture was simulated by applying downward gravitational forces on each FSU with patient-specific weight following anthropometric data [23, 24]. Springs were used to represent the action of the extensor muscles required to maintain the upright posture and counterbalance the patient's weight [11]. A bending moment of 5 Nm was then simulated to evaluate a typical functional upper-body flexion [25].

Model evaluation

To verify the computational modeling of the instrumentation and model calibration, the simulated correction maneuvers were compared to the actual postoperative radiographs using clinical indices (Cobb angle of the main curvature, T4–T12 kyphosis, and L1–L5 lordosis).

The validation, following ASME V&V40:2018 guidelines, was performed to assess the credibility of this biomechanical model in a previous study [15]. To this, the computed loads corresponding to PJF indicators for a group of asymptomatic patients and patients who have developed acute collapse PJF were compared. The sagittal moment at the adjacent spinal unit was found to discriminate the loads involved in the proximal segment when comparing both simulated groups. A sensitivity analysis and uncertainty quantification highlighted that the mechanical indices used to analyze PJF risks were within physiological ranges for the asymptomatic simulated group [15].

To assess the credibility of the sublaminar bands model, representative experiments of this surgical setting with SB and PS were simulated and compared to the reported data [9]. Five different spinal segments (T7–L2) were instrumented with different implant configurations: 1) PS from L2 to T10, 2) preceding configuration plus bilateral SB at T9 ("1-level SB") and 3) preceding configuration plus bilateral SB at T8 and T9 ("2-levels SB"). The caudal vertebra was fixed in space and a pure 4 Nm moment for the intact segment and 6 Nm for the instrumented configurations were applied to the cranial vertebra in flexion and in extension. The simulated SB were tensioned using a 350 N force. The intervertebral range of motion (iROM) between UIV and UIV + 2 following the flexion/extension was computed and expressed as a percentage of the motion of the uninstrumented spine configuration (% of intact motion) [9].

Design of experiment to test different proximal instrumentation stiffness fixations

Using a full-factorial design of experiments (DOE), 15 different rod stiffness and vertebra–rod fixation configurations were simulated for each of the 6 cases and 3 simulated phases (i.e., intraoperative instrumentation, postoperative erected posture, and 5 Nm flexion) by combining:

- UIV implant type: PS, SH, PS with sublaminar bands at the adjacent level with low (SB-50 N) [25] and high tensions (SB-250 N and SB-350 N) [26];
- Rod stiffness: high (CoCr, 6 mm diameter), medium (CoCr, 5.5 mm), and low (Ti, 5.5 mm).

Several dependent variables were computed to assess the risks of PJF. The proximal junctional angle (PJA), as well as the loads (i.e., forces and moments) held by the proximal anterior functional spinal units (FSU) were chosen as indicators of potential soft tissues disruption. The computed loads at the UIV implant–vertebra interface were used to estimate the risk of bone compaction or screw pull-out [11]. The bending and torsion moment held by the rods at the UIV level were chosen as indicators of rod breakage risk (Fig. 2). These biomechanical variables were post-processed and analyzed using non-parametric Kruskal–Wallis statistical tests for each of the 90 simulations (15 configurations × 6 cases) with Statistica software (TIBCO® Statistica). The results are presented in terms of median, minimum, and maximum for the flexion phase.

Results

Model evaluation

The mean difference between the simulated and actual postoperative instrumentation correction was of 2–3° for the regional curve angles, and 4° for the more local PJA angle (Table 2) for the six simulated cases, which is below the reported accuracy threshold corresponding to clinically relevant differences derived from 3D reconstructions from biplanar radiographs [27].

Compared to reported experiments for similar implant configurations, the simulated iROM using the SB and PS models were in general within 15% [9] (Table 3). For instance, the simulated flexion with 1-level SB was in good agreement with the in vitro study with an iROM reduction by 54% at UIV + 1 compared to PS (vs. 53% in the reference study [9]).

Design of experiment study of different proximal instrumentation stiffness fixations

The tension of the bands pulled the UIV + 1 toward the rod and the PJA was reduced on average by 2.3°, 5.5°, and 5.3° for the tensions of 50, 250, and 350 N, respectively,

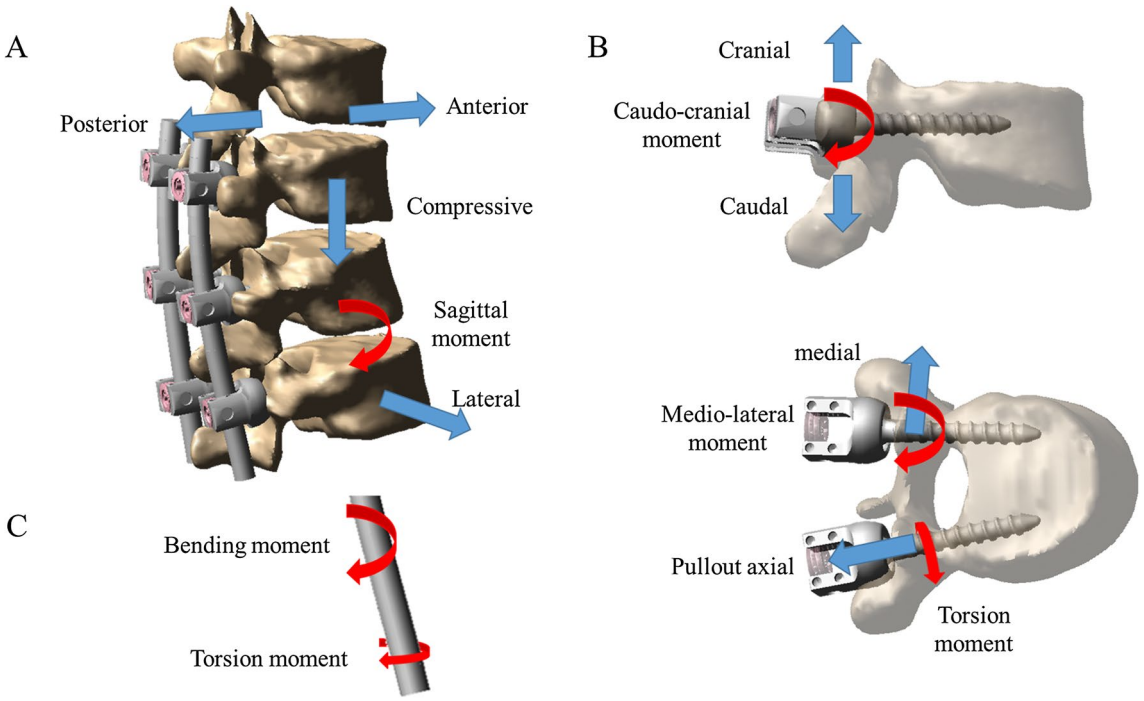

Fig. 2 Mechanical loads associated with risks of PJF in **A** functional spinal unit, **B** implant–vertebra connection, and **C** rod

Table 2 Simulated vs. actual postoperative correction

	Cobb angle of the main curvature (°)			T4–T12 kyphosis (°)			L1–L5 lordosis (°)			PJA (°)		
Case no	Actual	Simulated	Diff	Actual	Simulated	Diff	Actual	Simulated	Diff	Actual	Simulated	Diff
1	10	7	− 3	73	76	3	34	31	− 2	33	31	− 2
2	7	6	− 1	67	68	2	34	29	− 5	34	30	− 5
3	8	11	3	52	55	3	25	29	3	26	23	− 3
4	7	9	2	63	64	1	30	32	2	26	22	− 4
5	1	1	0	54	56	2	35	32	− 3	28	24	− 4
6	0	3	2	59	57	− 2	31	32	1	32	27	− 4
Mean difference (absolute value)			2			2			3			4

compared to PS, while the simulations with the simulated PJA with SH were reduced by 1.4° ($p > 0.05$). (Figs. 3 and 4).

The sagittal moment at UIV + 1 was significantly decreased with higher tension SB (SB-250 N and SB-350 N) as compared to PS (1.3 Nm and 2.5 Nm vs. 15.6 Nm, respectively), but it was significantly increased at UIV + 2 (17.7 Nm and 17.7 Nm vs. 15.5 Nm ($p < 0.05$). Low tension SB (SB-50 N) allowed a smoother load transition by decreasing a lesser amount of the moment at the UIV + 1 (8.1 Nm vs. 15.6 Nm, $p > 0.05$) and slightly increasing it at UIV + 2 (16.8 Nm vs. 15.5 Nm, $p > 0.05$). Using SH instead of PS at the UIV did not change the loads held by the proximal junctional spinal segment (PJSS) (Fig. 5).

SH significantly increased the caudo-cranial and torsion moments at the bone-implant interface compared to PS (2.6 Nm vs. 0.7 Nm; 2.7 Nm vs. 1.0 Nm, $p < 0.05$) (Table 4). SB with low tension (SB-50 N) had no impact on the loads held by the implant nor the rods at UIV compared to PS. With increased tension SB (SB-250 N and 350 N), the medio-lateral force at the bone-implant interface increased compared to PS (238 N and 297 N vs. 65 N, $p < 0.05$). It also decreased the pullout force compared to PS but thus increased the compression force on the bone-implant interface (− 237 N and − 236 N vs. − 14 N, $p < 0.05$). The

Table 3 Effect of sublaminar bands vs. pedicle screws only on intervertebral range of motion (iROM) after 6 Nm flexion and extension: published experimental tests of Viswanthan et al. compared to same simulations with our model (% difference of iROM)

	Flexion		Extension	
	[Viswanathan et al. 2019]	Simulation	[Viswanathan et al. 2019]	Simulation
T8–T9 (UIV + 2)				
SB-1 level	− 4	3	− 6	0
SB-2 levels	62	52*	58	48*
T9–T10 (UIV + 1)				
SB-1 level	53 *	54*	61	46
SB-2 levels	74 *	86*	75*	72*
T10–T11 (UIV)				
SB-1 level	− 11	13	− 3	13
SB-2 levels	1.9	21*	9	26*

PS pedicle screws, *SB* sublaminar bands, *UIV* upper instrumented vertebra (*$p < 0.05$ vs. PS only)

torsional and sagittal bending moment held by the rods were increased with high tension rods for SB-250 N and 350 N, respectively (5.2 Nm and 6.1 Nm vs. 2.8 Nm, $p < 0.05$; 5.4 Nm and 5.7 Nm vs. 0.6 Nm, $p < 0.05$) (Table 4).

Using low-stiffness rods (Ti/5.5 mm) significantly reduced the PJA compared to CoCr/5.5 mm and 6 mm rods (20.0° vs. 24.5° vs. 23.3°, $p < 0.05$), as well as the caudo-cranial moment at the bone-implant interface (0.7 Nm vs. 0.9 Nm vs. 1.0 Nm, $p < 0.05$) without affecting the loads held by the rods and the anterior spine (Table 5).

Discussion

This biomechanical numerical study presents the impact of implant and rod stiffness configurations on load sharing at the proximal junctional level, which distinguishes itself from previous studies that mainly used iROM to evaluate different instrumentation techniques [5]. Compared to the experimental study by Viswanathan et al. [9], SB modeling was found to have similar quantitative effects on iROM compared to PS alone for the configuration SB-1 level in flexion with a maximum difference of less than 0.5°, considered negligible.

The biomechanical simulations did not show any difference in FSU loading between the simulated SH and PS. While some clinical studies reported a lesser occurrence of PJK using hooks [28], this outcome is not consistent [29]. Our numerical study showed that SB smooth the loading transition, thus decrease the load gradient, between the instrumented and non-instrumented spine, which may reduce the risk of PJF. This transition, however, was influenced by the level of SB tension previously reported above 200 N [25]. The low-tension bands (SB-50 N) provided a more gradual transition through the PJSS in terms of iROM, as reported in [6, 7], but also for the sagittal moments held by the FSUs. This smoother transition may prevent proximal junctional acute collapse as seen in clinical studies [28, 30]. High-tension bands (SB-250 N and SB-350 N), on the other hand, decreased the moment at UIV + 1 but did not smooth the load distribution. The increased tension may decrease the

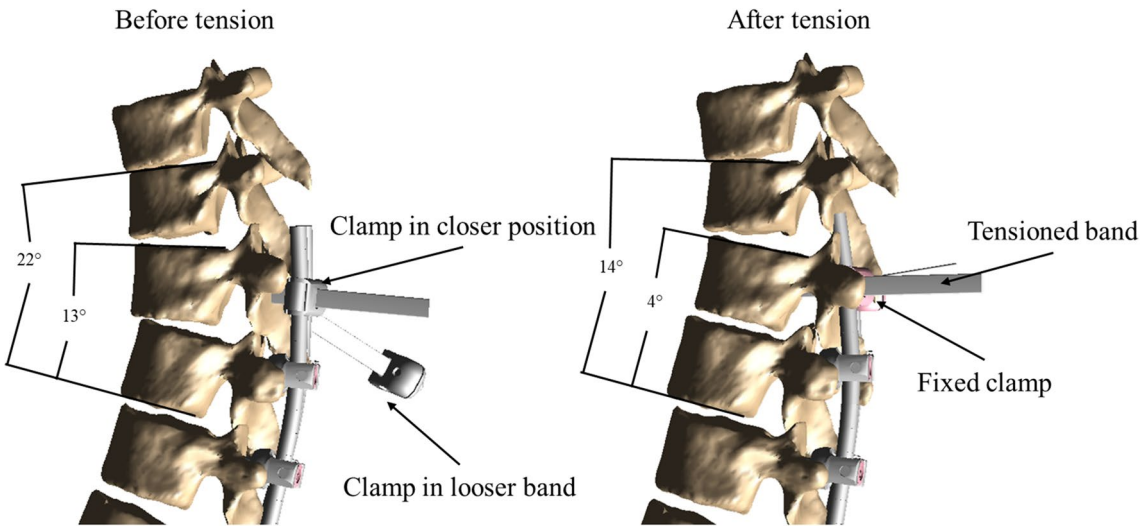

Fig. 3 Proximal junctional angle and UIV/UIV + 1 angle before and after 350 N tension of the sublaminar bands for a representative case (n°4)

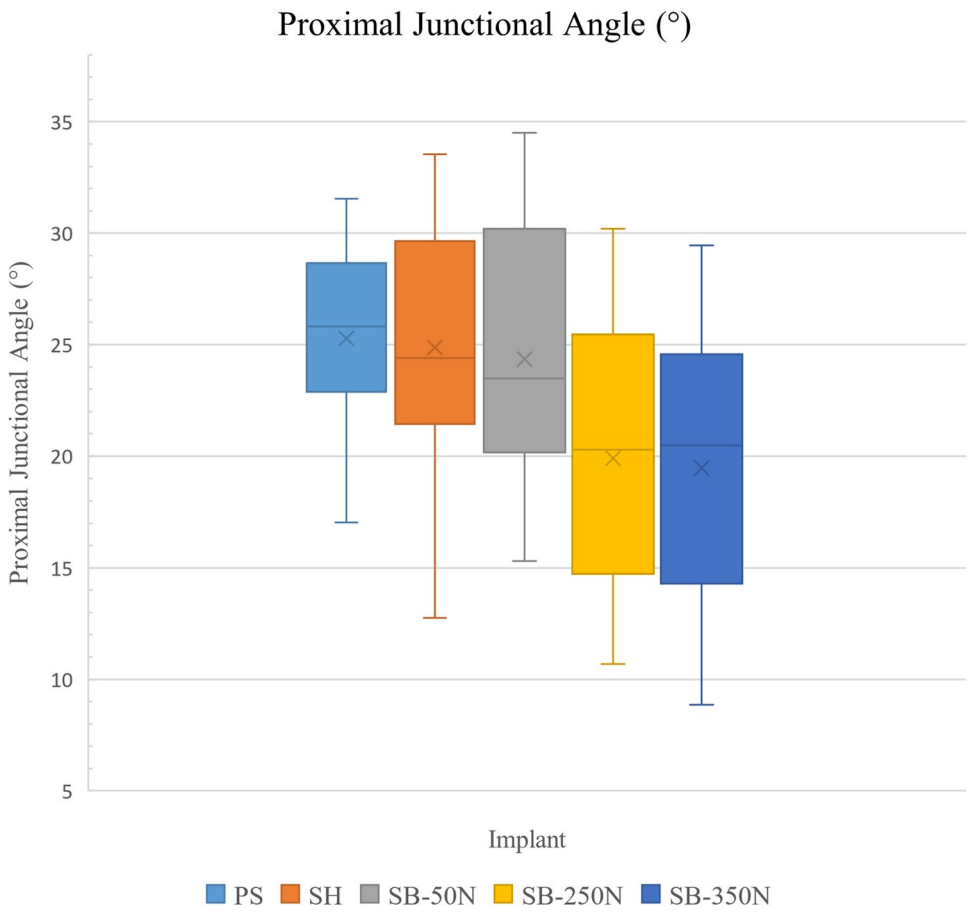

Fig. 4 PJA for different implant configurations measured after the simulated instrumentation (median, 25–75% values and min–max for the 18 simulations per implant type: 6 cases × 3 rod stiffnesses)

risk of acute collapse directly between the UIV and UIV + 1, but it could increase the risk of disruption cranially. Increasing the tension led to a significant increase of medio-lateral force and compression force at the bone-implant interface. The axial forces held by the bone-implant interface tend to be mainly compressive, but their variation also include pull-out forces. The order of magnitude of those forces could still be considered safe compared to the published evidence about pullout strength with different anchors [31]. Moreover, decreasing implant axial load to achieve more compression than pullout may be seen less risky in the context of PJF, where the implant–bone failure mode was predominantly reported in pullout. Increasing SB tension changed the load-sharing between the anterior spine and the instrumentation by releasing the sagittal moment on the FSU but increasing it at the rods level.

Using low-stiffness rods decreased the PJA compared to high stiffness rods, yet the impact of rod stiffness on the anterior spinal loading was not found. However, decreasing rod stiffness decreased the caudo-cranial moment held by the bone-implant interface without affecting the loads held by the rods themselves. Using Ti rods decreased the risk of bone compaction or PS failure and proximal collapse compared to CoCr rods. Considering their ultimate strength value, it also increased the risk of rod breakage since the loads on the rods remain similar. Clinical studies similarly reported that Ti rods reduce the risk of PJK, but with an increased number of cases of rod fracture [32] compared to CoCr rods, which are more prone to PS fracture and PJK [33].

This computational study has potential limitations that should be recognized. Even if the numerical model was comprehensively validated for relative assessment of surgical strategies against PJF risks, the simulated mechanical loads should be interpreted on their relative effect rather than their absolute values [15]. Although the six cases used in this study reflect some of the variability encountered in terms of spinal deformities, the small number limits the generalizability of the current study. Nevertheless, it must be kept in perspective that the objective of the study was to systematically analyze the first-order influence of the different instrumentation variables in play related to PJF at UIV using a parametric study, which resulted in a large number of simulations (90) to compare and evaluate their effects. The load gradient reduction between the instrumented and proximal uninstrumented spine as a biomechanical factor indicative of PJF risk [4] remains to be correlated with clinical cases.

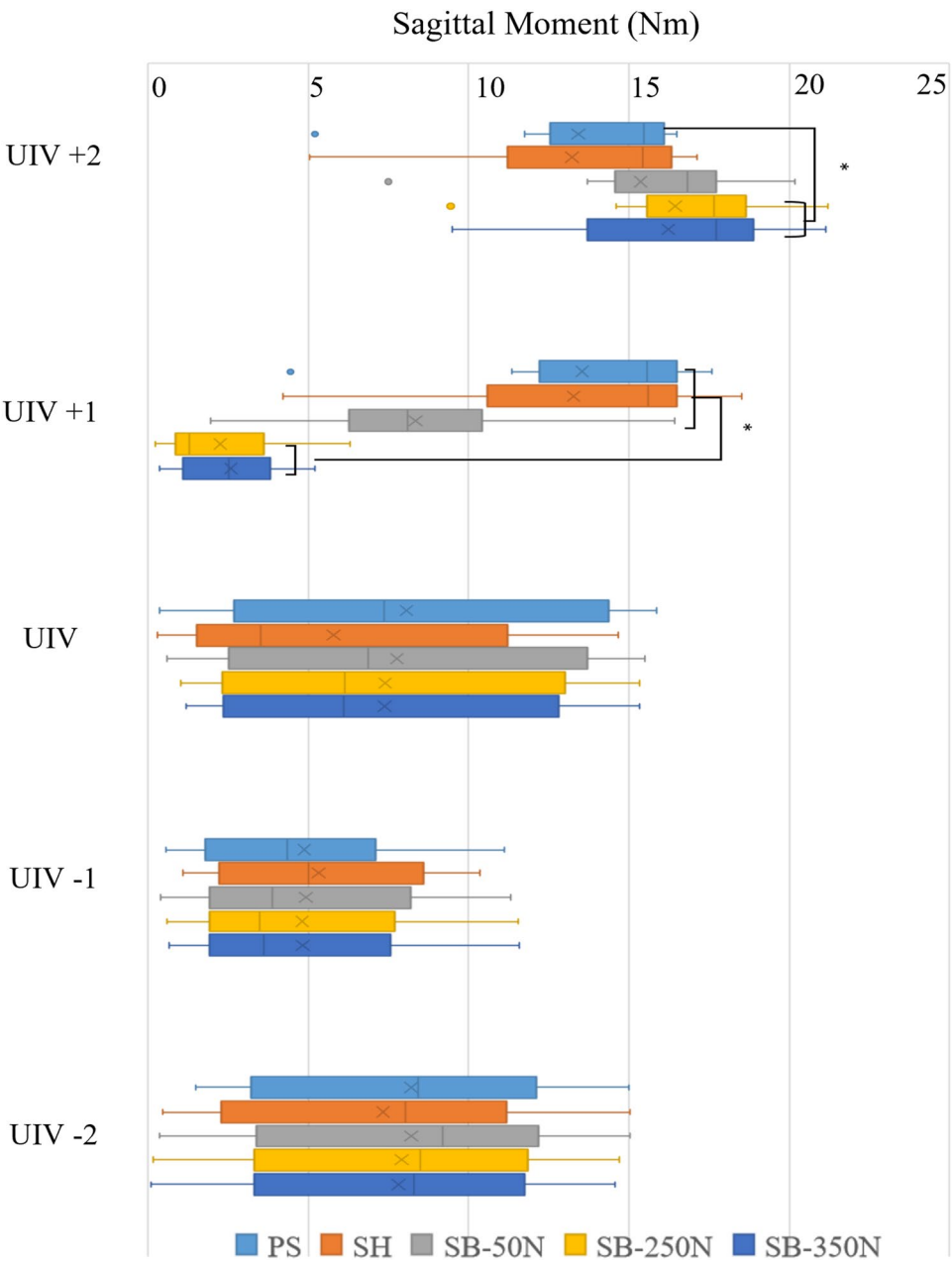

Fig. 5 Sagittal moment (in Nm) held by the functional spinal units around the proximal junction for different implant types (*$p < 0.05$)

Based on this biomechanical analysis, the ideal combination of rod–vertebra anchor depended on several factors. In these computational models, using less-stiff rods decreased the risk of implant failure, but not in combination with high tension SB due to the risk of rod breakage. For the simulated cases requiring correction of a relatively high thoracolumbar junction kyphosis, high tension SB combined with high stiffness rods addressed the needed correction. The rod contouring to the native regional kyphosis between the UIV and UIV-2 would also be expected to decrease the PJK risk post-op. The rod curvature around the UIV was also a consideration since the combination of CoCr rods with high tension SB may increase the risk of failure one level cranial to the instrumentation. The possibility of establishing a more gradual transition of loads, as allowed by SBs with low tension, is a biomechanically interesting avenue to mitigate the risk of PJF, which remains to be studied in greater detail in clinical practice.

Conclusions

This study biomechanically evaluated the effects of different proximal fixations and instrumentation stiffnesses on load-sharing in specific ASD cases, allowing the inference

Table 4 Simulated loads at the proximal junctional segment (illustrated in Fig. 2) after 5 Nm flexion for all implant types at UIV

	PS		SH		SB-50 N		SB-250 N		SB-350 N	
	Median	[min; max]	Median	[min; max]	Median	[min; max]	Median	[min; max]	Median	[min; max]
FSU										
UIV + 1										
Sagittal moment (Nm)	15.6	[4.5; 17.6]	15.6	[4.2; 18.5]	8.1	[2.0; 16.4]	1.3*	[0.2; 6.3]	2.5*	[0.4; 5.2]
UIV										
Postero-anterior force (N)	− 15	[− 220; 150]	− 110	[− 343; − 17]	28	[− 180; 179]	113	[− 135; 250]	134	[− 122; 279]
Medio-lateral force (N)	− 72	[− 126; 25]	− 37	[− 105; 78]	− 79	[− 122; 16]	− 72	[− 121; 14]	− 67	[− 120; 17]
Compressive force (N)	367	[93; 488]	316	[114; 479]	376	[178; 480]	245	[48; 417]	204	[50; 407]
Sagittal moment (Nm)	7.4	[0.4; 15.9]	3.5	[0.3; 14.7]	6.9	[0.6; 15.5]	6.1	[1.0; 15.3]	6.1	[1.2; 15.3]
Implants at UIV										
Caudo-cranial force (N)	149	[75; 464]	235	[92; 378]	122	[63; 466]	126	[49; 415]	135	[21; 395]
Medio-lateral force (N)	65	[17; 92]	69	[32; 163]	94	[57; 133]	238*	[164; 307]	297*	[97; 378]
Axial pullout force (N)	− 14	[− 106; 88]	− 94	[− 177; 183]	− 122	[− 244; 60]	− 237*	[− 360; − 127]	− 236*	[− 428; − 132]
Medio-lateral moment (Nm)	3.9	[1.6; 7.3]	3.5	[0.2; 6.0]	4.0	[1.8; 8.3]	4.8	[2.8; 8.3]	5.1	[1.7; 8.6]
Caudo-cranial moment (Nm)	0.7	[0.2; 1.1]	2.6*	[0.7; 5.4]	0.8	[0.4; 6.7]	0.8	[0.3; 1.8]	0.9	[0.1; 1.8]
Torsion moment (Nm)	1.0	[0.5; 2.1]	2.7*	[0.9; 5.9]	1.3	[0.4; 2.6]	1.5	[1.2; 3.7]	1.8*	[0.8; 4.0]
Rods at UIV										
Torsion moment (Nm)	2.8	[1.2; 5.1]	4.0	[1.8; 6.6]	2.6	[0.5; 4.6]	5.2*	[3.7; 6.1]	6.1*	[2.7; 8.8]
Bending moment (Nm)	0.6	[0.4; 2.3]	2.0	[0.5; 4.6]	2.0	[0.9; 3.1]	5.4*	[3.3; 7.4]	5.7*	[3.4; 9.1]

PS pedicle screws, *SH* supralaminar hooks, *SB* sublaminar bands, *UIV* upper instrumented vertebra, *FSU* functional spinal unit (*$p < 0.05$ vs. PS)

Table 5 Simulated loads at the proximal junctional segment (illustrated in Fig. 2) after flexion for all types of simulated rods

	CoCr 6 mm		CoCr 5.5 mm		Ti 5.5 mm	
	median	[min; max]	median	[min; max]	median	[min; max]
FSU						
UIV + 1						
Sagittal moment (Nm)	6.7	[0.4; 18.5]	7.2	[0.8; 18.1]	5.7	[0.2; 17.7]
UIV						
Postero-anterior force (N)	10	[− 343; 234]	1	[− 343; 202]	52	[− 335; 279]
Medio-lateral force (N)	− 71	[− 114; 69]	− 72	[− 126; 34]	− 67	[− 105; 78]
Compressive force (N)	265	[51; 478]	276	[48; 488]	303	[78; 480]
Sagittal moment (Nm)	4.8	[0.6; 15.7]	4.9	[0.3; 15.9]	4.7	[0.4; 15.4]
Implants at UIV						
Caudo-cranial force (N)	131	[59; 464]	147	[78; 466]	125	[21; 462]
Medio-lateral force (N)	107	[17; 378]	98	[25; 365]	121	[28; 351]
Axial pullout force (N)	− 143	[− 417; 183]	− 141	[− 353; 183]	− 134	[− 428; 181]
Medio-lateral moment (Nm)	4.5	[0.5; 7.2]	4.8	[0.7; 8.6]	3.4	[0.2; 5.4]
Caudo-cranial moment (Nm)	1.0	[0.2; 6.7]	0.9	[0.2; 4.7]	0.7*	[0.1; 5.4]
Torsion moment (Nm)	1.6	[0.5; 5.3]	1.5	[0.5; 5.9]	1.8	[0.4; 4.0]
Rods at UIV						
Torsion moment (Nm)	4.5	[0.5; 8.7]	4.3	[0.5; 8.8]	3.7	[0.5; 7.3]
Bending moment (Nm)	2.7	[0.5; 8.7]	2.8	[0.5; 9.1]	2.6	[0.4; 7.0]

CoCr cobalt–chrome, *Ti* titanium, *UIV* upper instrumented vertebra, *FSU* functional spinal unit (*$p < 0.05$ vs. CoCr 6 mm)

of recommendations to consider reducing the risk of PJF. Simulated sublaminar bands at the proximal adjacent level of the instrumentation only with low pretension allow smoothing of the anterior load distribution without unproperly increasing the loads on the instrumentation. Decreasing the proximal rod stiffness also decreased the risk of bone failure but increased the risk of rod breakage.

Acknowledgements Project funded by the Natural Sciences and Engineering Research Council of Canada (Industrial Research chair with Medtronic of Canada). Special thanks to Nathalie Bourassa for her assistance with 3D reconstruction of the patients and Christiane Caouette for her advice during the modeling phase.

Author contributions MLP: design, acquisition, analysis, interpretation of data for the work, drafting, final approbation, agree to be accountable. LLB: analysis, interpretation of the data for the work, revising, final approbation, agree to be accountable. JR: design, interpretation of the data for the work, revising, final approbation, agree to be accountable. DC: interpretation of the data for the work, revising, final approbation, agree to be accountable. C-ÉA: design, interpretation of the data for the work, revising, final approbation, agree to be accountable.

Funding Project funded by the Natural Sciences and Engineering Research Council of Canada (Industrial Research Chair with Medtronic of Canada).

Declarations

Conflict of interest Maeva Lopez Poncelas: doctoral scholarship supported by the Natural Sciences and Engineering Research Council of Canada (Industrial Research Chair with Medtronic of Canada). Luigi La Barbera: TransMedTech Institute Postdoctoral Fellowship (Canada First Research Excellence Fund). Jeremy Rawlinson: scientist employed by Medtronic and member of the Orthopaedic Research Society board of directors. Dennis Crandall: royalties for medical device development from Medtronic (outside the scope of the current study). Carl-Éric Aubin: supported by the Natural Sciences and Engineering Research Council of Canada (Industrial Research Chair with Medtronic Canada and Discovery Grant).

Ethical approval Approval was obtained from the ethics committee of Polytechnique Montréal. The procedures used in this study adhere to the tenets of the Declaration of Helsinki.

References

1. Glattes RC, Bridwell KH, Lenke LG et al (2005) Proximal junctional kyphosis in adult spinal deformity following long instrumented posterior spinal fusion: incidence, outcomes, and risk factor analysis. Spine 30:1643–1649
2. Hart R, McCarthy I, O'Brien M et al (2013) Identification of decision criteria for revision surgery among patients with proximal junctional failure after surgical treatment of spinal deformity. Spine (Phila Pa 1976) 38:E1223-1227. https://doi.org/10.1097/BRS.0b013e31829fedde

3. York PJ, Kim HJ (2020) Recurrent proximal junctional kyphosis. Tech Orthop 36(1):20–24
4. Echt M, Ranson W, Steinberger J et al (2020) A systematic review of treatment strategies for the prevention of junctional complications after long-segment fusions in the osteoporotic spine. Glob Spine J. https://doi.org/10.1177/2192568220939902
5. Doodkorte RJ, Vercoulen TF, Roth AK et al (2021) Instrumentation techniques to prevent proximal junctional kyphosis and proximal junctional failure in adult spinal deformity correction—a systematic review of biomechanical studies. Spine J. https://doi.org/10.1016/j.spinee.2021.01.011
6. Bess S, Harris JE, Turner AW et al (2017) The effect of posterior polyester tethers on the biomechanics of proximal junctional kyphosis: a finite element analysis. J Neurosurg Spine 26:125–133. https://doi.org/10.3171/2016.6.SPINE151477
7. Lange T, Schmoelz W, Gosheger G et al (2017) Is a gradual reduction of stiffness on top of posterior instrumentation possible with a suitable proximal implant? A biomechanical study. Spine J 17:1148–1155. https://doi.org/10.1016/j.spinee.2017.03.021
8. Facchinello Y, Brailovski V, Petit Y et al (2015) Biomechanical assessment of the stabilization capacity of monolithic spinal rods with different flexural stiffness and anchoring arrangement. Clin Biomech (Bristol, Avon) 30:1026–1035. https://doi.org/10.1016/j.clinbiomech.2015.09.011
9. Viswanathan VK (2019) Biomechanical assessment of proximal junctional semi-rigid fixation in long-segment thoracolumbar constructs. J Neurosurg Spine. https://doi.org/10.3171/2018.7.SPINE18136
10. Natarajan RN (2018) Biomechanical analysis of a long-segment fusion in lumbar spine—a finite element model study. J Biomech Eng. https://doi.org/10.1115/1.4039989
11. Cammarata M, Aubin CE, Wang X et al (2014) Biomechanical risk factors for proximal junctional kyphosis: a detailed numerical analysis of surgical instrumentation variables. Spine (Phila Pa 1976) 39:E500-507. https://doi.org/10.1097/BRS.0000000000000222
12. Aubin CE, Cammarata M, Wang X et al (2015) Instrumentation strategies to reduce the risks of proximal junctional kyphosis in adult scoliosis: a detailed biomechanical analysis. Spine Deformity 3:211–218. https://doi.org/10.1016/j.jspd.2014.09.054
13. Nguyen NL, Kong CY, Hart RA (2016) Proximal junctional kyphosis and failure-diagnosis, prevention, and treatment. Curr Rev Musculoskelet Med 9:299–308. https://doi.org/10.1007/s12178-016-9353-8
14. Benoit D, Wang X, Crandall DG et al (2020) Biomechanical analysis of sagittal correction parameters for surgical instrumentation with pedicle subtraction osteotomy in adult spinal deformity. Clin Biomech 71:45–52
15. Lopez Poncelas M et al (2022) Credibility assessment of patient-specific biomechanical models to investigate proximal junctional failure in clinical cases with adult spine deformity using ASME V&V40 standard. Comput Methods Biomech Biomed Eng 25(5):543–553
16. Kadoury S, Cheriet F, Laporte C et al (2007) A versatile 3D reconstruction system of the spine and pelvis for clinical assessment of spinal deformities. Med Biol Eng Compu 45:591–602
17. Panjabi MM, Brand RA Jr, White AA III (1976) Three-dimensional flexibility and stiffness properties of the human thoracic spine. J Biomech 9:185–192
18. Gardner-Morse MG, Stokes I (2004) Structural behavior of human lumbar spinal motion segments. J Biomech 37:205–212
19. Salvi G, Aubin C-E, Le Naveaux F et al (2016) Biomechanical analysis of Ponte and pedicle subtraction osteotomies for the surgical correction of kyphotic deformities. Eur Spine J 25:2452–2460
20. La Barbera L, Larson AN, Aubin CE (2021) How do spine instrumentation parameters influence the 3D correction of thoracic adolescent idiopathic scoliosis? A patient-specific biomechanical study. Clin Biomech. https://doi.org/10.1016/j.clinbiomech.2021.105346
21. Cidambi KR, Glaser DA, Bastrom TP et al (2012) Postoperative changes in spinal rod contour in adolescent idiopathic scoliosis: an in vivo deformation study. Spine (Phila Pa 1976) 37:1566–1572. https://doi.org/10.1097/BRS.0b013e318252ccbe
22. Garner MD, Wolfe SJ, Kuslich SD (2002) Development and preclinical testing of a new tension-band device for the spine: the Loop system. Eur Spine J 11(Suppl 2):S186-191. https://doi.org/10.1007/s00586-002-0463-1
23. Pearsall DJ, Reid JG, Livingston LA (1996) Segmental inertial parameters of the human trunk as determined from computed tomography. Ann Biomed Eng 24:198–210
24. Kiefer A, Parnianpour M, Shirazi-Adl A (1997) Stability of the human spine in neutral postures. Eur Spine J 6:45–53
25. Mar DE, Clary SJ, Burton DC et al (2019) Biomechanics of prophylactic tethering for proximal junctional kyphosis: characterization of spinous process tether pretensioning and pull-out force. Spine Deform 7:191–196. https://doi.org/10.1016/j.jspd.2018.06.017
26. Cho SK, Caridi J, Kim JS et al (2018) Attenuation of proximal junctional kyphosis using sublaminar polyester tension bands: a biomechanical study. World Neurosurg 120:e1136–e1142. https://doi.org/10.1016/j.wneu.2018.08.244
27. Glaser DA, Doan J, Newton PO (2012) Comparison of 3-dimensional spinal reconstruction accuracy: biplanar radiographs with EOS versus computed tomography. Spine 37:1391–1397
28. Buell TJ, Mullin JP, Nguyen JH et al (2018) A novel junctional tether weave technique for adult spinal deformity: 2-dimensional operative video. Oper Neurosurg (Hagerstown). https://doi.org/10.1093/ons/opy148
29. Sebaaly A, Riouallon G, Obeid I et al (2018) Proximal junctional kyphosis in adult scoliosis: comparison of four radiological predictor models. Eur Spine J 27:613–621. https://doi.org/10.1007/s00586-017-5172-x
30. Battista C, Wild C, Kreul S et al (2018) Prevention of proximal junctional kyphosis & failure using sublaminar bands in a hybrid construct in pediatric kyphosis deformity. Int J Spine Surg 12:644–649. https://doi.org/10.14444/5080
31. Liljenqvist U, Hackenberg L, Link T et al (2001) Pullout strength of pedicle screws versus pedicle and laminar hooks in the thoracic spine. Acta Orthop Belg 67(2):157–163
32. Shega FD, Zhang H, Manini DR et al (2020) Comparison of effectiveness between cobalt chromium rods versus titanium rods for treatment of patients with spinal deformity: a systematic review and meta-analysis. Adv Orthop 2020:1–10. https://doi.org/10.1155/2020/8475910
33. Tan LA (2020) Commentary: failure types and related factors of spinopelvic fixation after long construct fusion for adult spinal deformity. Neurosurgery. https://doi.org/10.1093/neuros/nyaa489